Shadows of rotating wormholes

Rajibul Shaikh*

Tata Institute of Fundamental Research,

Homi Bhabha Road, Colaba, Mumbai 400005, India

Abstract

We study shadows cast by a certain class of rotating wormholes and point out the crucial role of a rotating wormhole throat in the formation of a shadow, a crucial point overlooking of which has resulted erroneous results in the earlier studies on shadows of the same class of rotating wormholes. We explore the dependence of the shadows on the spin of the wormholes. We compare our results with that of the Kerr black hole. With increasing values of the spin, the shapes of the wormhole shadows start deviating considerably from that of the black hole. Such considerable deviation, if detected in future observations, may possibly indicate the presence of a wormhole. In other words, the results obtained here indicate that, through the observations of their shadows, the wormholes which are considered in this work and have reasonable spin, can be distinguished from a black hole.

* rajibul.shaikh@tifr.res.in

I. INTRODUCTION

It is commonly believed that the suppermassive compact region at our galactic center as well as those at the centers of many other galaxies contain suppermassive black holes. However, direct evidence for the presence of a black hole requires actual detection of the event horizon. A number of tests have been proposed to confirm the presence of event horizons in these black hole candidates [1–3]. The evidence is strong but, of necessity [4], not conclusive. Typically, a black hole event horizon together with a set of unstable light rings (or a photon sphere in the case of a spherically symmetric, static black hole) present in the exterior geometry of a black hole, is expected to create a characteristic shadow-like image (a dark region over a brighter background) of the radiation emitted by an accretion flow around the black hole or of the photons emitted by nearby light sources. With the purpose of detecting this shadow at mm wavelengths in the image of the suppermassive compact object Sagittarius A* (Sgr A*) present at our galactic center, as well as in the image of that present at the nucleus of the nearby galaxy M87, the event horizon telescope (EHT) [5–7], an Earth-spanning millimeter-wave interferometer, is being constructed and has begun collecting data.

While the intensity map of an image depends on the details of the accretion process and the emission mechanisms, the boundary of the shadow is only determined by the spacetime metric itself, since it corresponds to the apparent shape of the photon capture orbits as seen by a distant observer. Shadows cast by different black holes have been studied by several researchers in the past, both theoretically and numerically. The shadow of the Schwarzschild black hole was studied by Synge [8] and Luminet [9]. Bardeen studied the shadow cast by the Kerr black hole [10] (see [11] also). Consequently, the shadow of a Kerr black hole and its different aspects (e.g. measurement of the spin parameter) have been studied by several authors [12–19]. The shadows cast by other black holes such as Reissner-Nordstrom black hole [20, 21], binary black hole [22, 23], Kerr-Newman black hole [24–26], Kerr black hole with scalar hair [27], Kerr-Sen black hole [28, 29], regular black holes [30–35], Einstein-Maxwell-dilaton-axion black hole [36], Kerr-Taub-NUT black hole [37], Kerr-Newman-NUT black holes [38], braneworld black hole [39], Kaluza-Klein dilaton black hole [40], Einstein-dilaton-Gauss-Bonnet black hole [41], non-Kerr black hole [42, 43] and five-dimensional black hole [44, 45] have been studied in the past. See [46] for a recent brief review on shadow.

The presence of a shadow, however, does not by itself prove that a compact object is necessarily a black hole. Other horizonless compact objects such as a hard surface [48], naked singularities [49–51] and non-rotating wormholes [52–55] can also cast similar shadows. In this work, we study shadows of rotating wormholes of Teo class [56]. Although, shadows cast by this class of wormholes have been studied earlier [57, 58], the results obtained in these works are erroneous since they overlooked the crucial role of a throat of a rotating wormhole in the shadow formation. In this work, we revisit the problem and obtain the correct shapes of the shadows cast by the rotating Teo wormholes. Other than shadows, several other observational aspects of wormholes such as electromagnetic signatures of accretion disks around wormholes [59–61] and gravitational lensing [62–72] have been studied in the past. It is also worth mentioning that, although wormholes in general relativity necessarily violate different energy conditions, it is not so in the case of modified gravity wormholes (see [73–86] and references therein for some recent examples).

The plan of the paper is as follows. In the next section, we briefly recall the rotating Teo wormhole spacetime. In Sec. III, we study null geodesics in the spacetime of a rotating Teo wormhole. We obtain the apparent shapes of shadows cast by the rotating wormholes in Sec. IV. We conclude in Sec. V with a summary of the key results.

II. THE ROTATING WORMHOLE SPACETIME

We start with the stationary, axisymmetric spacetime metric describing a rotating traversable wormhole of Teo class. The metric is given by [56]

$$ds^2 = -N^2 dt^2 + \frac{dr^2}{1-\frac{b}{r}} + r^2 K^2 \left[d\theta^2 + \sin^2\theta (d\varphi - \omega dt)^2\right], \tag{2.1}$$

where $-\infty < t < \infty$, and $r_0 \leq r < \infty$, $0 \leq \theta \leq \pi$ and $0 \leq \phi \leq 2\pi$ are spherical coordinates. The functions N, b, K, and ω depend on r and θ only such that it is regular on the symmetry axis $\theta = 0, \pi$ [56]. The spacetime describes two identical, asymptotically flat regions joined together at the throat $r = r_0 = b > 0$. The above metric is a rotating generalization of the static Morris-Thorne wormhole [87].

To ensure that there are no curvature singularities or event horizons, the analog redshift function N must be nonzero and finite everywhere (from the throat to the spatial infinity). Also, to avoid any curvature singularity at the throat and to satisfy the flare-out condition

at the throat, the shape function b must satisfy $\partial_\theta b|_{r=r_0} = 0$, $\partial_r b|_{r=r_0} < 1$ and $b \leq r$ [56]. The metric function K determines the area radius given by $R = rK$ and ω measures the angular velocity of the wormhole.

The metric functions N, K, b and ω can be chosen freely provided the above-mentioned regularity conditions are satisfied, thereby obtaining a particular case of the rotating Teo wormhole. A particular choice of the metric functions frequently used in the literature, is given by [57, 58, 60, 61]

$$N = \exp\left[-\frac{r_0}{r} - \alpha\left(\frac{r_0}{r}\right)^\delta\right], \quad b(r) = r_0\left(\frac{r_0}{r}\right)^\gamma,$$
$$K = 1, \quad \omega = \frac{2J}{r^3}, \tag{2.2}$$

where J is the angular momentum of the wormhole and α, δ and γ are real constants. In the case when $\gamma = 0$, we can write $r_0 = 2M$, M being the mass of the wormhole.

The rotating wormhole 2.1 may contain an ergoregion around its throat. An ergoregion is a region where $g_{tt} = -(N^2 - \omega^2 r^2 K^2 \sin^2\theta) \leq 0$. The boundary of the ergoregion, i.e., the ergosurface is given by $g_{tt} = 0$. For the metric 2.1, the ergosurface is given by

$$N^2 - \omega^2 r^2 K^2 \sin^2\theta = 0. \tag{2.3}$$

Figure 1 shows the ergoregion of a rotating wormhole for the choice of metric functions

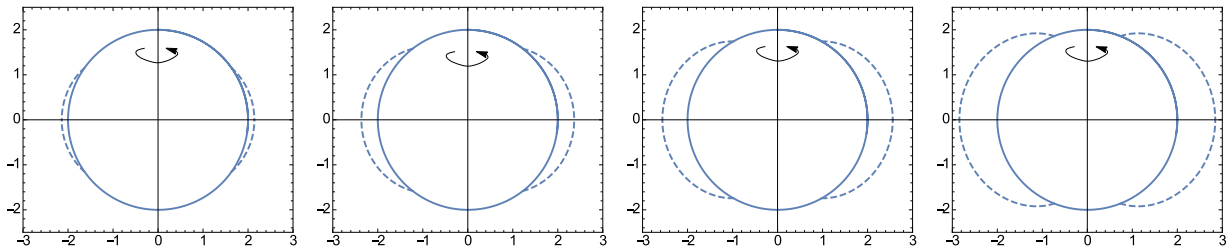

(a)$J/M^2 = 0.9$ (b)$J/M^2 = 1.2$ (c)$J/M^2 = 1.5$ (d)$J/M^2 = 2.0$

FIG. 1. The ergoregion of a rotating wormhole (in units of M) for the metric functions (2.2) with $\alpha = 0$, $\gamma = 0$ and $\delta = 0$. The region between the solid curve (wormhole throat) and the dashed curve (ergosurface) is the ergoregion. The arrow indicates the spin axis of the wormhole.

(2.2) with $\alpha = 0$, $\gamma = 0$ and $\delta = 0$. Note that the ergoregion does not extend upto the poles $\theta = 0$ and $\theta = \pi/2$. It exists between angles θ_c and $(\pi - \theta_c)$ (i.e., it touches the throat at these angles), where $0 < \theta_c \leq \pi/2$ and

$$\sin\theta_c = \left|\frac{N_0}{\omega_0 r_0 K_0}\right|. \tag{2.4}$$

In the above, the subscript '0' implies that the metric functions are evaluated at the throat. Also, note that the ergoregion exists when the spin a $(= J/M^2)$ crosses a certain critical value a_c given by $\sin\theta_c = 1$, i.e., by $\omega_c = \frac{N_0}{r_0 K_0}$. For the metric functions used in Fig. 1, the critical spin is given by $a_c = J_c/M^2 \simeq 0.74$.

III. NULL GEODESICS IN A ROTATING WORMHOLE SPACETIME

The Lagrangian describing the motion of a photon in the spacetime of the rotating wormhole (2.1) is given by

$$2\mathcal{L} = -N^2\dot{t}^2 + \frac{\dot{r}^2}{1-\frac{b}{r}} + r^2K^2\left[\dot{\theta}^2 + \sin^2\theta(\dot{\varphi}-\omega\dot{t})^2\right], \tag{3.1}$$

where an overdot represents a differentiation with respect to the affine parameter λ. Since the Lagrangian is independent of t and ϕ, we have two constants of motion, namely, the energy E and the angular momentum L (about the axis of symmetry) of the photon:

$$p_t = \frac{\partial\mathcal{L}}{\partial\dot{t}} = -N^2\dot{t} - \omega r^2K^2\sin^2\theta(\dot{\varphi}-\omega\dot{t}) = -E \tag{3.2}$$

$$p_\phi = \frac{\partial\mathcal{L}}{\partial\dot{\phi}} = r^2K^2\sin^2\theta(\dot{\varphi}-\omega\dot{t}) = L. \tag{3.3}$$

Solving last two equations, we obtain

$$\dot{t} = \frac{E-\omega L}{N^2}, \quad \dot{\varphi} = \frac{L}{r^2K^2\sin^2\theta} + \frac{\omega(E-\omega L)}{N^2}. \tag{3.4}$$

The r- and θ-component of the momentum are, respectively, given by

$$p_r = \frac{\partial\mathcal{L}}{\partial\dot{r}} = \frac{\dot{r}}{1-\frac{b}{r}}, \quad p_\theta = \frac{\partial\mathcal{L}}{\partial\dot{\theta}} = r^2K^2\dot{\theta}. \tag{3.5}$$

The r- and θ-part of the geodesic equations can be obtained by solving the Hamilton-Jacobi equation

$$\frac{\partial S}{\partial\lambda} = -\frac{1}{2}g^{\mu\nu}\frac{\partial S}{\partial x^\mu}\frac{\partial S}{\partial x^\nu}, \tag{3.6}$$

where S is the Jacobi action. If there is a separable solution, then in terms of the already known constants of the motion, it must take the form

$$S = \frac{1}{2}\mu^2\lambda - Et + L\varphi + S_r(r) + S_\theta(\theta), \tag{3.7}$$

where μ is the mass of the test particle. For photons, $\mu = 0$. If the metric functions N, b, K, and ω of the rotating wormhole (2.1) are functions of the radial coordinates r only, then

the Hamilton-Jacobi equation is separable. Inserting Eq. (3.7) into Eq. (3.6) and separating out the r- and θ-part, we obtain [57]

$$\left(\frac{dS_\theta}{d\theta}\right)^2 = \mathcal{K} - L^2\frac{\cos^2\theta}{\sin^2\theta}, \tag{3.8}$$

$$\left(1-\frac{b}{r}\right)N^2\left(\frac{dS_r}{dr}\right)^2 = (E-\omega L)^2 - \mu^2 N^2 - (\mathcal{K}+L^2)\frac{N^2}{r^2K^2}, \tag{3.9}$$

where $\mathcal{K}$ is the Carter constant. Note that the separation constant $\mathcal{K}$ is different from that chosen in [57]. $\mathcal{K}$ is related to the separation constant Q taken in [57] through $Q = \mathcal{K} + L^2$. Redefinition of the constant will not affect the shadow structures. We have chosen the constant in such a way that $\mathcal{K} = 0$ for geodesics which completely lie in the equatorial plane $\theta = \pi/2$. Since $p_r = \frac{\partial S}{\partial r} = \frac{dS_r}{dr}$ and $p_\theta = \frac{\partial S}{\partial \theta} = \frac{dS_\theta}{d\theta}$, using Eqs. (3.5), (3.8), and (3.9), we obtain

$$\frac{N}{\left(1-\frac{b}{r}\right)^{1/2}}\frac{dr}{d\lambda} = \pm\sqrt{R(r)}, \quad r^2K^2\frac{d\theta}{d\lambda} = \pm\sqrt{T(\theta)}, \tag{3.10}$$

where

$$R(r) = (E-\omega L)^2 - \mu^2N^2 - (\mathcal{K}+L^2)\frac{N^2}{r^2K^2}, \tag{3.11}$$

$$T(\theta) = \mathcal{K} - L^2\frac{\cos^2\theta}{\sin^2\theta}. \tag{3.12}$$

Although, there are three constants of motions E, L and $\mathcal{K}$, the geodesic motion of a photon is characterised by two independent parameters defined by

$$\xi = \frac{L}{E}, \quad \eta = \frac{\mathcal{K}}{E^2}. \tag{3.13}$$

ξ and η are known as impact parameters. By introducing a new affine parameter $\tilde{\lambda} = E\lambda$, we can redefine the functions $R(r)$ and $T(\theta)$ as

$$R(r) = (1-\omega\xi)^2 - (\eta+\xi^2)\frac{N^2}{r^2K^2}, \quad T(\theta) = \eta - \frac{\xi^2}{\sin^2\theta}, \tag{3.14}$$

where we have taken $\mu = 0$ for a photon.

For latter use, we write down the radial equation of motion in the following form:

$$\left(\frac{dr}{d\tilde{\lambda}}\right)^2 + V_{eff} = 0, \quad V_{eff} = -\frac{1}{N^2}\left(1-\frac{b}{r}\right)R(r), \tag{3.15}$$

where V_{eff} is the effective potential describing the geodesic motion of a photon.

IV. SHADOWS OF ROTATING WORMHOLES

A wormhole connects two regions of spacetime. To obtain the shadow cast by a wormhole, we assume that the wormhole is illuminated by a light source situated in one of the regions, and no light sources are present in the vicinity of the throat in the other region [57]. Depending on the impact parameters, some of the photons from the light source plunge into the wormhole, pass through the throat and go to the other region, and some get scattered away to the infinity of the first region. A distant observer situated in the first region only receives the scattered photons. Therefore, in the observer's sky, the scattered photons form bright spots, whereas the photons captured by the wormhole form dark spots. The union of the dark spots in the observer's sky constitute the shadow.

Therefore, the task is to find out the critical orbits that separate the escaping and plunging photons. These critical orbits are characterised by certain critical values of the impact parameters ξ and η. A small perturbation in these critical values can turn it either to an escape or to a capture orbit. Therefore, the critical impact parameters define the boundary of a shadow. The critical orbits are unstable circular photon orbits corresponding to the highest maximum of the effective potential V_{eff}. The unstable circular photon orbits are determined by the standard conditions

$$V_{eff} = 0, \quad \frac{dV_{eff}}{dr} = 0, \quad \frac{d^2V_{eff}}{dr^2} \leq 0. \tag{4.1}$$

Note that, while writing the above set conditions in terms of $R(r)$, one must be careful about the throat where $(1 - \frac{b}{r}) = 0$ (see Eq. 3.15). For the unstable circular orbits whose radii do not coincide with the throat radius r_0 (i.e. for the unstable circular orbits lying outside the throat such that $(1 - \frac{b}{r}) \neq 0$ on the circular orbits), in terms of $R(r)$, the above set of conditions can be written as

$$R(r) = 0, \quad \frac{dR}{dr} = 0, \quad \frac{d^2R}{dr^2} \geq 0. \tag{4.2}$$

Using $R = 0$ and $dR/dr = 0$, we obtain [57]

$$\eta = \left[\frac{r^2K^2}{N^2}(1 - \omega\xi)^2 - \xi^2\right]_{r=r_{ph}}, \tag{4.3}$$

$$\xi = \frac{\Sigma}{\Sigma\omega - \omega'}\Big|_{r=r_{ph}}, \quad \Sigma = \frac{1}{2}\frac{d}{dr}\ln\left(\frac{N^2}{r^2K^2}\right), \tag{4.4}$$

where r_{ph} is the radius of a circular photon orbit. The authors in [57] used the above set of equations for ξ and η to obtain the shadows. But, they overlooked the fact that the effective potential can exhibit extremum at the wormhole throat, thereby implying circular photon orbits (either stable or unstable) at the throat. For example, for a non-rotating wormhole, the wormhole throat acts as the position of the maximum of the potential when there are no extrema outside the throat, thereby the throat being the position of unstable circular orbits and hence deciding the boundary of a shadow [52, 53]. In our case, since $(1-\frac{b}{r})$ vanishes at the throat $r=r_0$, it can be seen from (3.15) that the effective potential have a maximum, i.e., Eq. (4.1) is satisfied at the throat when

$$R(r_0)=0, \quad \frac{d^2R}{dr^2}\Big|_{r=r_0}\geq 0, \tag{4.5}$$

which is different from (4.2). For circular photon orbits at the throat, we have $R(r_0)=0$, i.e.,

$$(1-\omega_0\xi)^2-(\eta+\xi^2)\frac{N_0^2}{r_0^2K_0^2}=0, \tag{4.6}$$

where the subscript '0' implies that the functions are evaluated at the throat.

For a given metric functions and metric parameter values, the parametric plot of (4.3) and (4.4) with respect to the parameter r_{ph} plus the plot of (4.6) define the boundary of a shadow in the impact parameter space. However, in realistic observation, the apparent shape of a shadow is measured in the observer's sky, a plane passing through the center of the wormhole and normal to the line of sight joining the observer and the center of the wormhole. The coordinates on this plane are denoted by α and β and are known as celestial coordinates.

In terms of the tangent to a photon geodesic at the observer's position, the celestial coordinates are given as [88]

$$\alpha=\lim_{r\to\infty}\left(-r^2\sin\theta_{obs}\frac{d\varphi}{dr}\right), \quad \beta=\lim_{r\to\infty}r^2\frac{d\theta}{dr}, \tag{4.7}$$

where θ_{obs} is the inclination angle, i.e., the angle between the rotation axis of the wormhole and the line of sight of the observer. Using the geodesic equations, we obtain

$$\alpha=-\frac{\xi}{\sin\theta_{obs}}, \quad \beta=\left(\eta-\xi^2\frac{\cos^2\theta_{obs}}{\sin^2\theta_{obs}}\right)^{1/2}. \tag{4.8}$$

In the (α,β)-plane, Eqs. (4.3), (4.4) and (4.8) define the part of the boundary of the shadow formed by the unstable circular photon orbits which lie outside the throat. However, for

the part of the boundary of the shadow which is due to the unstable circular orbits at the throats, we have, from Eqs. (4.6) and (4.8),

$$(N_0^2 - \omega_0^2 r_0^2 K_0^2 \sin^2\theta_{obs})\alpha^2 - 2\omega_0 r_0^2 K_0^2 \sin\theta_{obs}\alpha - r_0^2 K_0^2 + N_0^2\beta^2 = 0. \tag{4.9}$$

The authors in [57] didn't consider the above-mentioned contribution of the throat in the shadow formation. Therefore, the results they obtained are incomplete and erroneous. The correct and complete results are obtained when one consider the last equation as well. To show it explicitly, we consider the following metric functions:

$$N = \exp\left[-\frac{r_0}{r}\right], \quad b(r) = r_0 = 2M, \quad K = 1, \quad \omega = \frac{2J}{r^3}. \tag{4.10}$$

In Fig. 2, we have plotted an example of a shadow for the metric parameter values corre-

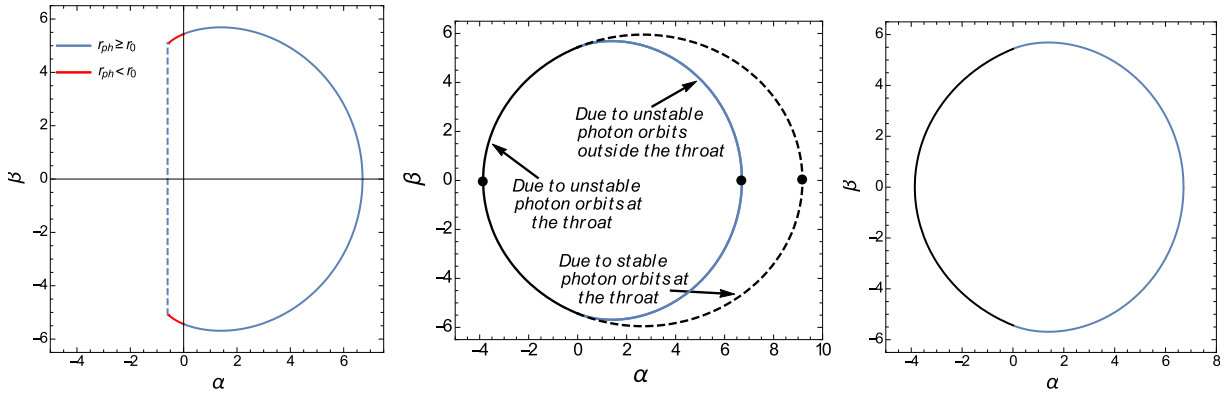

(a) (b) (c)

FIG. 2. Plots showing how the shape of a shadow looks like when the contribution of the throat (Eq. 4.9) (a) is not and (b) is considered. Here, the metric functions are given by (4.10) and J/M^2=0.3. (c) shows the actual shape of the shadow. The vertical dashed line in (a) is drawn by hand. The impact parameters denoted by the black dots are used in Fig. 3(a).

sponding to the third figure in the first row of Fig. 1 of [57]. The corresponding shadow obtained without considering the contribution of the throat, i.e., without considering Eq. 4.9 (which is the case in [57]) is shown in Fig. 2(a). When the contribution of the throat is taken into consideration, we obtain Fig. 2(b). The correct shape of the shadow shown in Fig. 2(c), is given by the common region enclosed by the curve obtained from Eqs. (4.3), (4.4) and (4.8) (the blue curve in Fig. 2(b)) and the curve obtained from Eq. (4.9) (the black curve in Fig. 2(b)). Moreover, from the red part of the plot in Fig. 2(a), it seems

that, while plotting the parametric plot using (4.3), (4.4) and (4.8), the authors in [57] have considered $r_{ph} < r_0$ also, which is not correct since the wormhole spacetime is valid only for $r \geq r_0$.

The reason why the shadow is given by the common region enclosed by the curves mentioned above, can be understood as follows. A circular photon orbit (stable or unstable) with given critical impact parameters lies in a plane which passes through the center of the wormhole and makes an angle θ_{ph} with the rotation axis, where $T(\theta_{ph}) = 0$. If, in a given plane, there are no stable and unstable photon orbits outside the throat, then the throat acts as a position of the unstable photon orbit, i.e., the potential has a maximum at the throat. The solid black curve in Fig. 2(b) corresponds to this situation. However, in a given plane, if there are stable or unstable photon orbits, then the throat acts as a position of either stable or unstable photon orbits. Figure 2(b) shows that, in the case where there is a unstable photon orbit (solid blue curve) outside the throat, the throat acts as the the position of a stable photon orbit (dashed black curve). To elaborate it further, we choose different values of α and β (which is equivalent of choosing ξ and η) and plot the effective potential. However, to show the effective potential for both the regions of the wormhole, we use the proper radial distance given by [87]

$$l(r) = \pm \int_{r_0}^{r} \frac{dr}{\sqrt{1 - \frac{b}{r}}}, \tag{4.11}$$

where the plus sign corresponds to one region and the minus sign to the other region. The throat is at $l(r_0) = 0$.

Figure 3(a) shows the plots of the effective potential for the parameter values denoted by the black dots shown in Fig. 2(b). It is clear that, for the impact parameter values denoted by the black dot on the solid black, solid blue and black dashed curve of Fig. 2(b), respectively, we have an unstable photon orbit at the throat, an unstable photon orbit outside the throat and a stable photon orbit at the throat, which are in agreement with Fig. 2(b). Also, note that the critical impact parameters corresponding to the stable orbits at the throat can not decide the boundary of a shadow since photons (with these impact parameters) from the distant source get turned away from some l (r) where $V_{eff} = 0$, before they reach the throat (see the black dashed plot of Fig. 3(a)). Figures 3(b)) and 3(c)), respectively, shows the plots of the effective potential for impact parameter values lying inside and outside of the shadow boundary of Fig. 2(c)). Note that, since the effective potential does not have any turning

point (i.e. $V_{eff} \neq 0$) for the impact parameter lying inside the shadow boundary, photons with these impact parameters plunge into the wormhole, pass through the throat and go to the other side (see Fig. 3(b)). These photons are not received by the distant observer, thereby creating dark spots in the observer's sky. On the other hand, the effective potential always have a turning point (i.e. $V_{eff} = 0$) at some l (r) for the impact parameter values lying outside the shadow boundary (see Fig. 3(c)). Photons with these impact parameter escape to the distant observer, thereby creating bright spots in the observer's sky. This explains why the correct shape of the shadow is given by the common region enclosed by the blue and black curves of Fig. 2(b)).

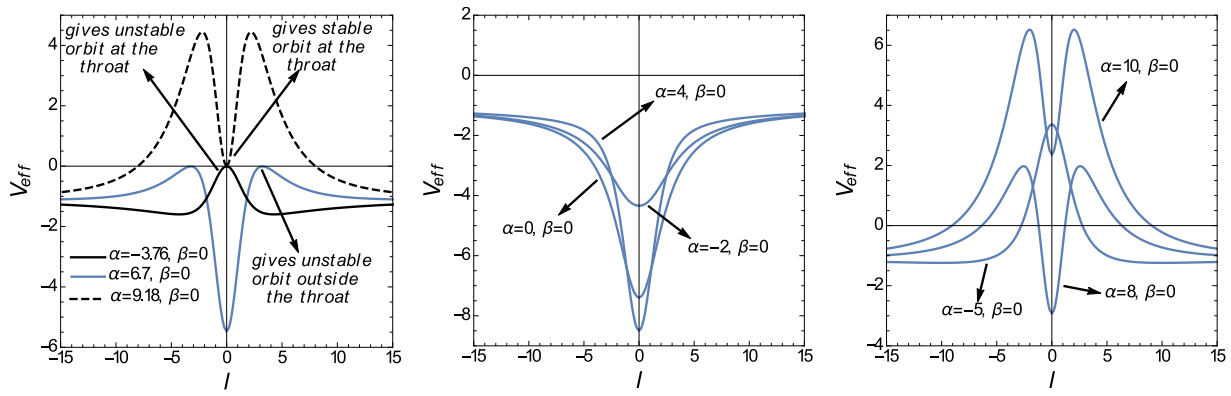

(a) (b) (c)

FIG. 3. Plots of the effective potential for (a) impact parameter values denoted by the black dots of Fig. 2(b) and for those lying (b) inside and (c) outside of the shadow boundary shown in Fig. 2(c). Here, $\theta_{obs} = \pi/2$. Corresponding values of ξ and η can be calculated from Eq. (4.8).

With the above discussions in mind, we now obtain the apparent shape of the shadow cast by a rotating wormhole. Figures (4) and (5) show the shadow cast by a rotating wormhole whose metric functions are given by (4.10). For each set of the parameter values, we have also plotted the shadow cast by a Kerr black hole for comparison. Note that, for small spin a ($= J/M^2$), the wormhole shadow is qualitatively similar to that of the Kerr black hole, i.e., they both are almost circular. However, with increasing values of the spin, the characteristic deformation of the shadow (i.e., deviation from the circular shape) due to the spin is more and more prominent in the wormhole case than that in the black hole case. Such considerable deviation of the wormhole shadow from that of the Kerr black hole may be relevant to discriminate between the wormhole and the black hole in future observations.

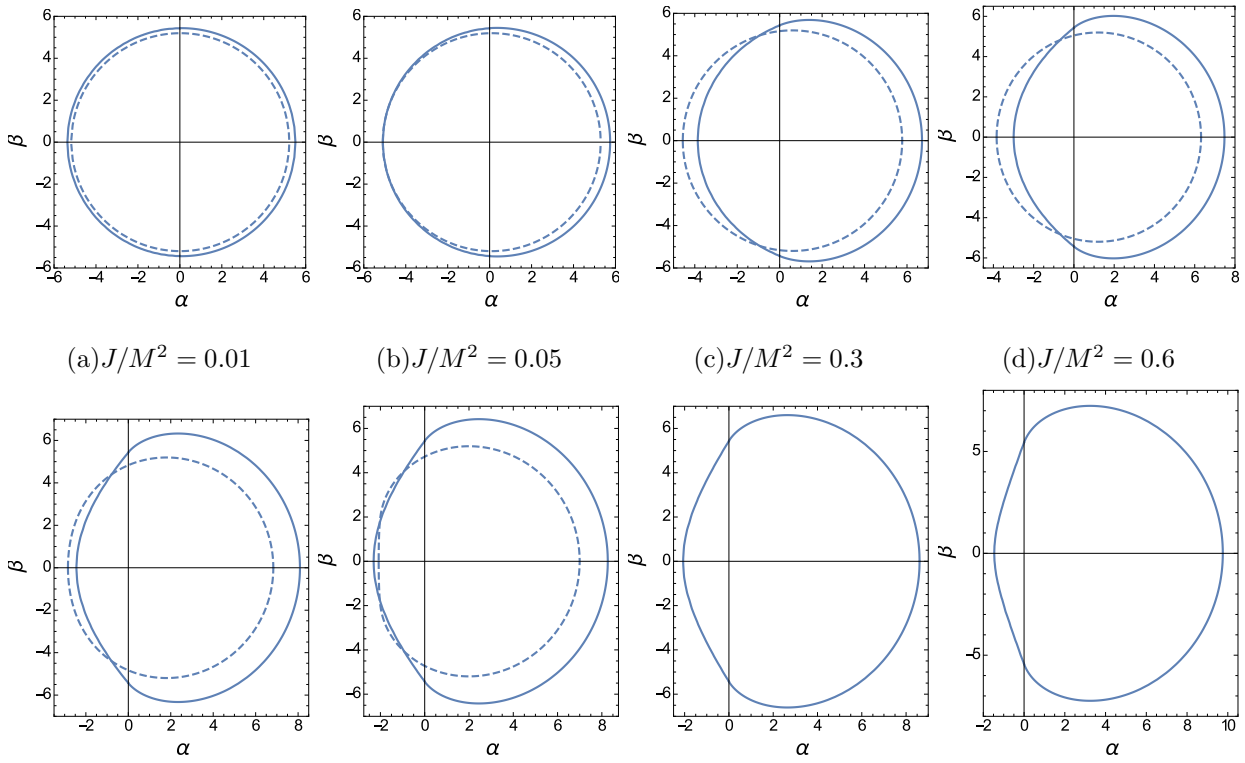

(a)$J/M^2 = 0.01$ (b)$J/M^2 = 0.05$ (c)$J/M^2 = 0.3$ (d)$J/M^2 = 0.6$

(e)$J/M^2 = 0.9$ (f)$J/M^2 = 1.0$ (g)$J/M^2 = 1.2$ (h)$J/M^2 = 2.0$

FIG. 4. The shadow of a rotating wormhole (solid curve) whose metric functions are given by (4.10) and the Kerr black hole (dashed curve) for different spin values. Here, $\theta_{obs} = 90°$. The axes are in units of the mass M.

As a second example, we consider a wormhole whose metric functions are given by

$$N = \exp\left[-\frac{r_0}{r} - \frac{r_0^2}{r^2}\right], \quad b(r) = r_0 = 2M, \quad K = 1, \quad \omega = \frac{2J}{r^3}. \tag{4.12}$$

The shadow for the above choice of the metric functions, along with that of the Kerr black hole, are shown in Fig. 6 for different values of the spin parameter. In this case, the shadow of the wormhole is larger than that of the black hole for all spin. Also, note that, similar to the earlier case, in this case too, the wormhole shadow start deviating from the black hole one as we increase the spin.

V. CONCLUSION

In this work, we have studied shadows cast by rotating wormholes. We have discussed in details why and how the throat of a rotating wormhole plays crucial role in the shadow

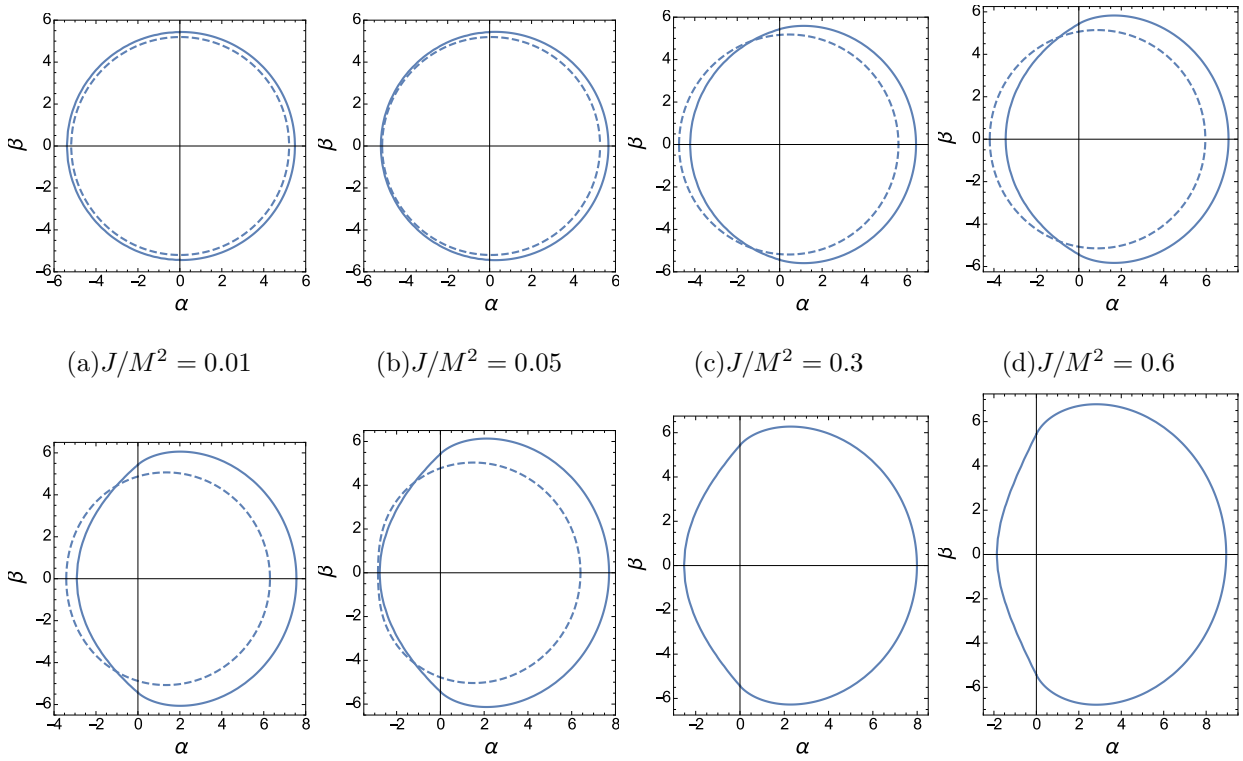

(a)$J/M^2 = 0.01$ (b)$J/M^2 = 0.05$ (c)$J/M^2 = 0.3$ (d)$J/M^2 = 0.6$

(e)$J/M^2 = 0.9$ (f)$J/M^2 = 1.0$ (g)$J/M^2 = 1.2$ (h)$J/M^2 = 2.0$

FIG. 5. The shadow of a rotating wormhole (solid curve) whose metric functions are given by (4.10) and the Kerr black hole (dashed curve) for different spin values. Here, $\theta_{obs} = 45^{\circ}$. The axes are in units of the mass M.

formation. This crucial role of the throat has been overlooked in the earlier studies [57, 58] on shadow of the same class of rotating wormholes considered here. Therefore, the results obtained in the above-mentioned earlier works are incomplete and erroneous. We have revisited the problem and obtained the correct shapes of the shadows. We have compared our results with that of the Kerr black hole. For small spin, the wormhole shadow is qualitatively similar to that of the Kerr black hole, i.e., they both are almost circular. However, with increasing values of the spin, the shapes of the wormhole shadows start deviating considerably from that of the black hole. Such considerable deviation, if detected in future observations, may possibly indicate the presence of a wormhole. In other words, the results obtained here indicate that, through the observations of their shadows, a wormhole having reasonable spin, can be distinguished from a black hole.

However, our conclusions are largely based on the types of wormholes we have chosen to work with. It will be interesting to see whether or to what extent the conclusions drawn

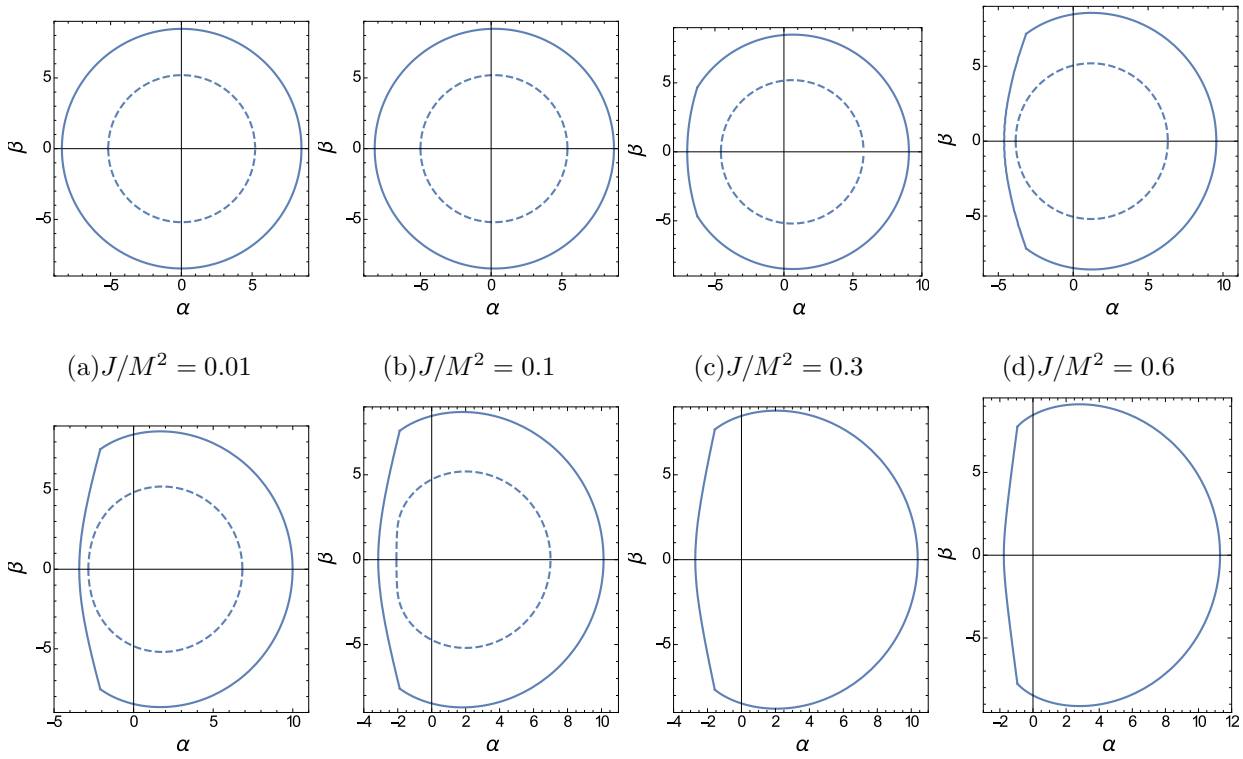

(a)$J/M^2 = 0.01$ (b)$J/M^2 = 0.1$ (c)$J/M^2 = 0.3$ (d)$J/M^2 = 0.6$

(e)$J/M^2 = 0.9$ (f)$J/M^2 = 1.0$ (g)$J/M^2 = 1.2$ (h)$J/M^2 = 2.0$

FIG. 6. The shadow of a rotating wormhole (solid curve) whose metric functions are given by (4.12) and the Kerr black hole (dashed curve) for different spin values. Here, $\theta_{obs} = 90°$. The axes are in units of the mass M.

here carry over to a broader class of rotating wormholes.

[1] A. E. Broderick, A. Loeb, and R. Narayan, *The event horizon of Sagittarius A**, ApJ **701**, 1357 (2009).

[2] A. E. Broderick, R. Narayan, J. Kormendy, E. S. Perlman, M. J. Rieke, and S. S. Doeleman, *The event horizon of M87*, ApJ **805**, 179 (2015).

[3] R. Narayan and J. E. McClintock, *Advection-dominated accretion and the black hole event horizon*, New Astron. Rev. **51**, 733 (2008).

[4] M. A. Abramowicz, W. Kluzniak, and J.-P. Lasota, *No observational proof of the black-hole event-horizon*, A&A, **396**, L31 (2002).

[5] S. S. Doeleman et al., *Event-horizon-scale structure in the supermassive black hole candidate*

at the Galactic Centre, Nature **455**, 78 (2008).

[6] S. S. Doeleman et al., *Jet-Launching Structure Resolved Near the Supermassive Black Hole in M87*, Science **338**, 355 (2012).

[7] `http://www.eventhorizontelescope.org.`

[8] J. L. Synge, *The escape of photons from gravitationally intense stars*, Mon. Not. R. Astron. Soc. **131**, 463 (1966).

[9] J.-P. Luminet, *Image of a spherical black hole with thin accretion disk*, Astron. Astrophys. **75**, 228 (1979).

[10] J. M. Bardeen, in *Black Holes (Les Astres Occlus)*, edited by C. Dewitt and B. S. Dewitt (Gordon and Breach, 1973), pp. 215-239.

[11] S. Chandrasekhar, *The Mathematical Theory of Black Holes* (Oxford University Press, New York, 1998).

[12] H. Falcke, F. Melia, and E. Agol, *Viewing the shadow of the black hole at the galactic center*, Astrophys. J. **528**, L13 (2000).

[13] R. Takahashi, *Shapes and positions of black hole shadows in accretion disks and spin parameters of black holes*, Astrophys. J. **611**, 996 (2004).

[14] A. F. Zakharov, A. A. Nucita, F. De Paolis, and G. Ingrosso, *Measuring the black hole parameters in the galactic center with RADIOASTRON*, New Astron. **10**, 479 (2005).

[15] K. Hioki and K.-I. Maeda, *Measurement of the Kerr spin parameter by observation of a compact object's shadow*, Phys. Rev. D **80**, 024042 (2009).

[16] F. De Paolis, G. Ingrosso, A. A. Nucita, A. Qadir, and A. F. Zakharov, *Estimating the parameters of the Sgr A^* black hole*, Gen. Relativ. Gravit. **43**, 977 (2011).

[17] K. Beckwith and C. Done, *Extreme gravitational lensing near rotating black holes*, Mon. Not. R. Astron. Soc. **359**, 1217 (2005).

[18] A. E. Broderick and A. Loeb, *Frequency-dependent shift in the image centroid of the black hole at the galactic center as a test of general relativity*, Astrophys. J. **636**, L109 (2006).

[19] R. Takahashi and K. Y. Watarai, *Eclipsing light curves for accretion flows around a rotating black hole and atmospheric effects of the companion star*, Mon. Not. R. Astron. Soc. **374**, 1515 (2007).

[20] A. F. Zakharov, F. De Paolis, G. Ingrosso, and A. A. Nucita, *Direct measurements of black hole charge with future astrometrical missions*, Astron. Astrophys. **442**, 795 (2005).

[21] A. F. Zakharov, *Constraints on a charge in the Reissner-Nordstrom metric for the black hole at the Galactic Center*, Phys. Rev. D **90**, 062007 (2014).

[22] A. Yumoto, D. Nitta, T. Chiba, and N. Sugiyama, *Shadows of multi-black holes: Analytic exploration*, Phys. Rev. D **86**, 103001 (2012).

[23] J. O. Shipley and S. R. Dolan, *Binary black hole shadows, chaotic scattering and the Cantor set*, Class. Quantum Grav. **33** (2016) 175001.

[24] P. J. Young, *Capture of particles from plunge orbits by a black hole*, Phys. Rev. D **14**, 3281 (1976).

[25] A. de Vries, *The apparent shape of a rotating charged black hole, closed photon orbits and the bifurcation set A_4*, Classical Quantum Gravity **17**, 123 (2000).

[26] R. Takahashi, *Black Hole Shadows of Charged Spinning Black Holes*, Publ. Astron. Soc. Jpn. 57, 273 (2005).

[27] P. V. P. Cunha, C. A. R. Herdeiro, E. Radu, and H. F. Runarsson, *Shadows of Kerr Black Holes with Scalar Hair*, Phys. Rev. Lett. **115**, 211102 (2015).

[28] K. Hioki and U. Miyamoto, *Hidden symmetries, null geodesics, and photon capture in the Sen black hole*, Phys. Rev. **D78**, 044007 (2008).

[29] S. Dastan, R. Saffari, and S. Soroushfar, *Shadow of a Kerr-Sen dilaton-axion Black Hole*, arXiv:1610.09477.

[30] Z. Li and C. Bambi, *Measuring the Kerr spin parameter of regular black holes from their shadow*, J. Cosmol. Astropart. Phys. **01** (2014) 041.

[31] A. Abdujabbarov, M. Amir, B. Ahmedov, and S. G. Ghosh, *Shadow of rotating regular black holes*, Phys. Rev. D **93**, 104004 (2016).

[32] M. Amir and S. G. Ghosh, *Shapes of rotating nonsingular black hole shadows*, Phys. Rev. D **94**, 024054 (2016).

[33] M. Sharif and S. Iftikhar, *Shadow of a charged rotating non-commutative black hole*, Eur. Phys. J. C **76**, 630 (2016).

[34] N. Tsukamoto, *Black hole shadow in an asymptotically-flat, stationary, and axisymmetric spacetime: The Kerr-Newman and rotating regular black holes*, Phys.Rev. D **97**, 064021 (2018).

[35] A. Saha, M. Modumudi, and S. Gangopadhyay, *Shadow of a noncommutative geometry inspired Ayon Beato Garcia black hole*, arXiv:1802.03276.

[36] S. W. Wei and Y. X. Liu, *Observing the shadow of Einstein-Maxwell-Dilaton-Axion black hole*,

J. Cosmol. Astropart. Phys. **11** (2013) 063.

[37] A. Abdujabbarov, F. Atamurotov, Y. Kucukakca, B. Ahmedov, and U. Camci, *Shadow of Kerr-Taub-NUT black hole*, Astrophys. Space Sci. **344**, 429 (2013).

[38] A. Grenzebach, V. Perlick, and C. Lammerzahl, *Photon regions and shadows of Kerr-Newman-NUT black holes with a cosmological constant*, Phys. Rev. D **89**, 124004 (2014).

[39] L. Amarilla and E. F. Eiroa, *Shadow of a rotating braneworld black hole*, Phys. Rev. D **85**, 064019 (2012).

[40] L. Amarilla and E. F. Eiroa, *Shadow of a Kaluza-Klein rotating dilaton black hole*, Phys. Rev. D **87**, 044057 (2013).

[41] P. V. P. Cunha, C. A. R. Herdeiro, B. Kleihaus, J. Kunz, and E. Radu, *Shadows of Einstein-dilaton-Gauss-Bonnet black holes*, Phys. Lett. B **768** (2017) 373.

[42] F. Atamurotov, A. Abdujabbarov, and B. Ahmedov, *Shadow of rotating non-Kerr black hole*, Phys. Rev. D **88**, 064004 (2013).

[43] M. Wang, S. Chen, and J. Jing, *Shadow casted by a Konoplya-Zhidenko rotating non-Kerr black hole*, JCAP **10** (2017) 051.

[44] U. Papnoi, F. Atamurotov, S. G. Ghosh, and B. Ahmedov, *Shadow of five-dimensional rotating Myers-Perry black hole*, Phys. Rev. D **90**, 024073 (2014).

[45] M. Amir, B. P. Singh, and S. G. Ghosh, *Shadows of rotating five-dimensional EMCS black holes*, arXiv:1707.09521.

[46] P. V. P. Cunha and C. A. R. Herdeiro, *Shadows and strong gravitational lensing: a brief review*, arXiv:1801.00860.

[47] P. V. P. Cunha, C. A. R. Herdeiro, and M. J. Rodriguez, *Does the black hole shadow probe the event horizon geometry?*, arXiv:1802.02675.

[48] A. E. Broderick and R. Narayan, *On the nature of the compact dark mass at the galactic center*, Astrophys. J. **638**, L21 (2006).

[49] C. Bambi and K. Freese, *Apparent shape of super-spinning black holes*, Phys. Rev. D **79**, 043002 (2009).

[50] N. Ortiz, O. Sarbach, and T. Zannias, *Shadow of a naked singularity*, Phys. Rev. D **92**, 044035 (2015).

[51] R. Shaikh, P. Kocherlakota, R. Narayan, and P. S. Joshi, *Shadows of spherically symmetric black holes and naked singularities*, arXiv:1802.08060.

[52] C. Bambi, *Can the supermassive objects at the centers of galaxies be traversable wormholes? The first test of strong gravity for mm/sub-mm very long baseline interferometry facilities*, Phys. Rev. D **87**, 107501 (2013).

[53] T. Ohgami and N. Sakai, *Wormhole shadows*, Phys. Rev. D **91**, 124020 (2015).

[54] M. Azreg-Ainou, *Confined-exotic-matter wormholes with no gluing effect– Imaging supermassive wormholes and black holes*, J. Cosmol. Astropart. Phys. **7**, 37 (2015).

[55] T. Ohgami and N. Sakai, *Wormhole shadows in rotating dust*, Phys. Rev. D **94**, 064071 (2016).

[56] E. Teo, *Rotating traversable wormholes*, Phys. Rev. D **58**, 024014 (1998).

[57] P. G. Nedkova, V. Tinchev, and S. S. Yazadjiev, *Shadow of a rotating traversable wormhole*, Phys. Rev. D **88**, 124019 (2013).

[58] A. Abdujabbarov, B. Juraev, B. Ahmedov, and Z. Stuchlik, *Shadow of rotating wormhole in plasma environment*, Astrophys. Space Sci. **361**, (2016) 226.

[59] T. Harko, Z. Kovacs, and F. Lobo, *Electromagnetic signatures of thin accretion disks in wormhole geometries*, Phys. Rev. D **78**, 084005 (2008).

[60] T. Harko, Z. Kovacs, and F. Lobo, *Thin accretion disks in stationary axisymmetric wormhole spacetimes*, Phys. Rev. D **79**, 064001 (2009).

[61] C. Bambi, Broad Kα iron line from accretion disks around traversable wormholes, Phys. Rev. D **87**, 084039 (2013).

[62] J. G. Cramer, R. L. Forward, M. S. Morris, M. Visser, G. Benford, and G. A. Landis, *Natural wormholes as gravitational lenses*, Phys. Rev. D **51**, 3117 (1995).

[63] M. Safonova, D. F. Torres, and G. E. Romero, *Microlensing by natural wormholes: Theory and simulations*, Phys. Rev. D **65**, 023001 (2001).

[64] K. K. Nandi, Y.-Z. Zhang, and A. V. Zakharov, *Gravitational lensing by wormholes*, Phys. Rev. D **74**, 024020 (2006).

[65] F. Abe, *Gravitational microlensing by the Ellis wormhole*, Astrophys. J. **725**, 787 (2010).

[66] K. Nakajima and H. Asada, *Deflection angle of light in an Ellis wormhole geometry*, Phys. Rev. D **85**, 107501 (2012).

[67] N. Tsukamoto, T. Harada, and K. Yajima, *Can we distinguish between black holes and wormholes by their Einstein-ring systems?*, Phys. Rev. D **86**, 104062 (2012).

[68] N. Tsukamoto and T. Harada, *Light curves of light rays passing through a wormhole*, Phys. Rev. D **95**, 024030 (2017).

[69] R. Shaikh and S. Kar, *Gravitational lensing by scalar-tensor wormholes and the energy conditions*, Phys. Rev. D **96**, 044037 (2017).

[70] K. Jusufi, A. Ovgun, *Gravitational lensing by rotating wormholes*, Phys. Rev. D **97**, 024042 (2018).

[71] K. Jusufi, N. Sarkar, F. Rahaman, A. Banerjee, and S. Hansraj, *Deflection of light by black holes and massless wormholes in massive gravity*, arXiv:1712.10175.

[72] K. Jusufi, A. Ovgun, A. Banerjee, and I. Sakalli, *Gravitational lensing by wormholes supported by electromagnetic, scalar, and quantum effects*, arXiv:1802.07680.

[73] H. Maeda and M. Nozawa, *Static and symmetric wormholes respecting energy conditions in Einstein-Gauss-Bonnet gravity*, Phys. Rev. D **78**, 024005 (2008).

[74] F. S. N. Lobo and M. A. Oliveira, *Wormhole geometries in f(R) modified theories of gravity*, Phys. Rev. D **80**, 104012 (2009).

[75] M. H. Dehghani and S. H. Hendi, *Wormhole solutions in Gauss-Bonnet-Born-Infeld gravity*, Gen. Relativ. Gravit. **41**, 1853 (2009).

[76] P. Kanti, B. Kleihaus, and J. Kunz, *Wormholes in Dilatonic Einstein-Gauss-Bonnet Theory*, Phys. Rev. Lett. **107**, 271101 (2011).

[77] T. Harko, F. S. N. Lobo, M. K. Mak, and S. V. Sushkov, *Modified-gravity wormholes without exotic matter*, Phys. Rev. D **87**, 067504 (2013).

[78] R. Shaikh, *Lorentzian wormholes in Eddington-inspired Born-Infeld gravity*, Phys. Rev. D **92**, 024015 (2015).

[79] S. Kar, S. Lahiri, and S. SenGupta, *Can extra dimensional effects allow wormholes without exotic matter?*, Phys. Lett. B **750**, 319 (2015).

[80] K. A. Bronnikov and A. M. Galiakhmetov, *Wormholes without exotic matter in Einstein-Cartan theory*, Grav. Cosmol. **21**, 283 (2015).

[81] C. Bambi, A. Cardenas-Avendano, G. J. Olmo, and D. Rubiera-Garcia, *Wormholes and nonsingular space-times in Palatini f(R) gravity*, Phys. Rev. D **93**, 064016 (2016).

[82] R. Shaikh and S. Kar, *Wormholes, the weak energy condition, and scalar-tensor gravity*, Phys. Rev. D **94**, 024011 (2016).

[83] C. Menchon, G. J. Olmo, and D. Rubiera-Garcia, *Nonsingular black holes, wormholes, and de Sitter cores from anisotropic fluids*, Phys. Rev. D **96**, 104028 (2017).

[84] P. H. R. S. Moraes, R. A. C. Correa, and R. V. Lobato, *Analytical general solutions for static*

wormholes in f(R,T) gravity, JCAP **07**, 029 (2017).

[85] H. Moradpour, N. Sadeghnezhad, and S. H. Hendi, *Traversable asymptotically flat wormholes in Rastall gravity*, Can. J. Phys. **95**, 1257 (2017).

[86] M. Hohmann, C. Pfeifer, M. Raidal, and H. Veermae, *Wormholes in conformal gravity*, arXiv:1802.02184.

[87] M. S. Morris and K. S. Thorne, *Wormholes in spacetime and their use for interstellar travel: A tool for teaching general relativity*, Am. J. Phys. **56**, 395 (1988).

[88] S. E. Vazquez and E. P. Esteban, *Strong-field gravitational lensing by a Kerr black hole*, Nuovo Cimento Soc. Ital. Fis. **119B**, 489 (2004).